Results in Materials 22 (2024) 100555

Contents lists available at ScienceDirect

Results in Materials

journal homepage: www.sciencedirect.com/journal/results-in-materials

Fabrication and characterization of mesoporous calcium silicate and silver-incorporated mesoporous calcium silicate nanoparticles with low cytotoxicity and antibacterial properties as a dental biomaterial

Amer A. Mohammed [a], Ahmed H. Ali [b,*]

[a] Aesthetic and Restorative Dentistry, College of Dentistry, University of Baghdad, Baghdad, Iraq
[b] Aesthetic and Restorative Dentistry, College of Dentistry, University of Baghdad, Baghdad, Iraq

ARTICLE INFO

Keywords:
Mesoporous
Nanoparticles
Silver
Enterococcus faecalis
Mineralization

ABSTRACT

Aim: This study aimed to fabricate and characterize Mesoporous calcium silicate nanoparticles (MCSNs) and silver-incorporated Mesoporous calcium silicate nanoparticles (Ag-MCSNs) as bioactive nanoparticles either for hybridization with contemporary endodontic materials to improve their bioactivity by using (MCSNs) as a drug delivery system, and to achieve both low cytotoxicity and enhanced antibacterial activity by incorporating Ag which is avery potent antibacterial agent to form (Ag-MCSNs) as new multifunctional materials.

Methods: The MCSNs and Ag-MCSNs nanoparticles were made using the template method. Both nanoparticles' mesoporous structure, specific surface area, pore volume, pore size, and shape were examined and characterized by FTIR, XRD, EDS, DLS, and FE-SEM. The ion release, pH change, cytotoxicity by MTT assay, and antibacterial properties against planktonic *Enterococcus faecalis* were further investigated by colony forming units (CFUs) counting technique.

Result: MCSNs nanoparticles were prepared and successfully incorporated with silver as Ag-MCSNs. MCSNs and Ag-MCSN nanoparticles had the characteristic mesoporous material shape and over time showed sustained ion release (Ca^{2+},Si^{4+} and Ag^{+}) ,with an alkaline pH value (8.2–9.0). Both materials showed no obvious cytotoxicity but more cell viability with MCSNs (vitality value is >70%). Both nanoparticles showed antibacterial activity against *Enterococcus faecalis* ($p < 0.05$). With MCSNs containing Ag (Ag-MCSNs) showing higher antibacterial effect.

Conclusion: Both mesoporous calcium silicate nanoparticles (MCSNs) and mesoporous calcium silicate nanoparticles loaded with silver (Ag-MCSNs) displayed a characteristic mesoporous structure, ion release, alkaline pH, minimal cytotoxicity, and outstanding antibacterial performance with MCSNs containing Ag (Ag-MCSNs) showing higher antibacterial effect. This substance may be improved to provide a better root canal filler material, sealer, or novel intracanal medicament in dentistry.

1. Introduction

Nanomaterials are organic, inorganic, or artificial substances that comprise particles in aggregates, agglomerates, or free states, at least *50%* of which have exterior diameters ranges about 100 nm and 1 nm. These are categorized according to their origin, materials utilized, and size [1]. Outcome of their nanoscale dimensions and high surface/volume *ratio*, nanomaterials offer distinct benefits over their bulk counterparts in that they exhibit distinctive physicochemical features [2].

Antimicrobial nanoparticles can also penetrate biofilms more effectively and they are effective at lower doses and may help reduce the rising use of antibiotics. Nanoparticles can penetrate biofilms and electrostatically interact with bacterial cell membranes, which damages cell membranes, increases permeability, produces reactive oxygen species, impairs cellular processes, degrades proteins, damages DNA, and finally causes cell death [3]. Researchers have devoted considerable effort to the use of nanoparticles in root canal therapy over the past ten years. Our collective knowledge of this topic has significantly increased since its inception, and new studies are constantly expanding the body of existing information [4].

Due to the bioactivity of calcium silicate (CS) based materials, scaffolds containing different stem cells are now being built for tissue

* Corresponding author.
E-mail addresses: amergawad2015@uomustansiriyah.edu.iq (A.A. Mohammed), ahmed.ali@codental.uobaghdad.edu.iq (A.H. Ali).

https://doi.org/10.1016/j.rinma.2024.100555
Received 9 February 2024; Received in revised form 29 February 2024; Accepted 3 March 2024
Available online 8 March 2024

regeneration. They created a CS-based substance in earlier research that has subsequently been made available due to its alkalinity, as a valuable medical adjuvant, and capacity to generate apatite and antibacterial characteristics. The capacity to promote odontogenic and osteogenic differentiation in multiple cell types, including adipose-derived stem cells, stromal cells of bone marrow, dental pulp cells, and periodontal ligament cells, is another benefit of CS-based materials. However, this substance has shown two flaws: *first*, the particles of CS-based materials are often at the micrometer level, making injection problematic; *second*, standard CS-based materials have a small nanopore structure, drastically limiting the potential for drug administration [5].

Mesoporous materials have been employed in several prior investigations to demonstrate their potential as innovative drug delivery systems with controllable release kinetics [6]. Mesoporous materials are defined as having pores with diameters between 2 and 50 nm; they are smaller than microporous (50 nm) materials. Mesoporous materials with a physically well-ordered structure have been proposed as suitable carriers for biomolecule loading and controlled release. Targeted drug delivery is a crucial component of tumor therapy, and materials' bioactivity is crucial for fostering tissue regeneration. To mix with biomaterials for diverse bioengineering applications, such as intracellular molecule labeling, drug administration, and gene targeting, mesoporous CS (MCSNs) nanoparticles with a higher surface area have been produced [7]. Mesoporous calcium-silicate nanoparticles (MCSNs) are considered a superior biomaterial since they encourage stem cells to differentiate into osteoblasts and exhibit favorable apatite-mineralization characteristics in the apical area of the root canal. They serve as excellent delivery methods for pharmaceuticals, such as antibiotics and antibacterial compounds, since they feature highly organized channel mesopore architectures and further ideal pore volume and surface area [8]. Mesoporous CS nanoparticles (MCSNs) have the advantages of mesoporosity as well as the capacity to release Ca and Si ions in this regard [9]. Silver nanoparticles (AgNPs) have received a lot of attention in dental research. AgNPs have a multiple-level strategy, making them both antibacterial and antifungal [4]. AgNPs were demonstrated to have antibacterials against *E. faecalis* in the context of endodontic diseases. Yet, given their ability to stain and cause discoloration of the dentinal wall, in addition to the cosmetic outcome of endodontic therapy. However, AgNPs' propensity to agglomerate and cytotoxicity have both sparked controversy [10].

The desired features of root canal filling material should include broad-spectrum antibacterial behavior to suppress the growth of bacteria in the periapical area, excellent mineralization to facilitate sealing of the apical root canal of a tooth and enhance the integration between biomaterials and periapical tissues, and excellent osteogenic properties to promote hard tissue formation. For these reasons, it is very important to develop MCSNs with excellent apatite mineralization as well as osteogenic, drug delivery, and antibacterial characteristics for endodontic materials [5,11].

This study aimed to fabricate and characterize Mesoporous calcium silicate nanoparticles (MCSNs) and silver-incorporated Mesoporous calcium silicate nanoparticles (Ag-MCSNs) as bioactive nanoparticles either for hybridization with contemporary endodontic materials to improve their bioactivity, and to achieve both low cytotoxicity and enhanced antibacterial activity or as new multifunctional materials.

2. Materials and methods

2.1. Materials

Tetraethyl orthosilicate (TEOS) and Cetyltrimethylammonium bromide (CTAB) were acquired from (Sigma Aldrich Co. USA). Ammonium hydroxide, calcium nitrate tetrahydrate ($Ca(No_3)_2.4H_2O$), silver nitrate ($AgNO_3$), and Tris-HCL (1 M, pH7.4), originating from (Sinopharm Chemical Reagent Co. China).

2.2. Synthesis of MCSN and nanosilver-incorporated MCSN (Ag-MCSN)

According to Wu et al., 2012, MCSNs were synthesized utilizing a template technique [12]. Briefly, 600 mL of deionized or double-distilled water (ddH_2O) was used for dissolving CTAB (6.6 g), and then ammonium hydroxide was added dropwise (12 mL). After 30 min of stirring, calcium nitrate tetrahydrate (31.2 g) and TEOS (30 mL) were added. The mixture was well mixed for 3 h before being rinsed 3 times with double-distilled water (ddH_2O) and 100% ethanol, respectively. The powders were gathered, then dried in the oven at 60 °C for a whole night and then calcination was done at 550 °C on the stove for 2 h to remove any last remnants of CTAB. The same procedures were used to create nanosilver MCSNs (Ag-MCSNs) using the templated method, but 4,911 g of silver nitrate ($AgNO_3$) was added along with (31.2 g) of calcium nitrate tetrahydrate and 30 mL of TEOS. The powders that were obtained were given the name Ag-MCSNs. (Fig. 1).

2.3. Characterization of MCSN and Ag-MCSN

Chemical characterization of the MCSN, Ag-MCSN was obtained using Fourier-transform infrared spectroscopy (FTIR, Shimadzu FTIR-8400s spectrometer, Japan), x-ray diffraction (XRD, Shimadzu labX XRD-6000, Japan) and Energy dispersive spectrometry (EDS, SEM-FEI Inspect S 50, USA). Structural characterization was obtained by dynamic light scattering (DLS) with Particle's size analyzer (PSA, Brokhaven 90 Plus Nanoparticle Size Analyzer, USA), Brunauer-Emmett-Teller analysis (BET, Micromeritics ASAP 2020 Physisorption BET, USA) and field emission-scanning electron microscopy (FE-SEM, CSEM-FEG inspect F50, USA).

2.4. Ion release and pH evaluation of MCSN and Ag-MCSN

20 mg of MCSN and Ag-MCSN were soaked for 1, 3, and 9 days in 10 mL of Tris-HCl (1 M, pH 7.4) at 37 °C. Inductively coupled plasma-atomic emission spectrometry was employed to calculate the concentration of the released Ca ion (Ca^{2+}), Si ions (SiO_3^{-2}), and Ag^{+} at every instant using 5 mL of the solution (PlasmaQuant 9100 series ICP-AES, Analytik Jena, Germany). 5 mL of new Tris-HCl was added to the recovered solution. The total number of ions emitted from the Ag-MCSN and MCSN at each time point was determined. For MCSN and Ag-MCSN pH measurements, 150 mg of each substance were dissolved in 30 mL of ddH_2O at 37 °C. A pH meter (HI 2550 pH/ORP &EC/TDS/NaCL Meter, HANNA instrument, USA) was used to measure the pH change over time at 1, 3, 6, and 9 days.

2.5. Antibacterial effect of nanoparticles against E. faecalis

The antibacterial effects of both nanoparticles on *E. faecalis* (ATCC 29212; American Type Culture Collection (ATCC), Manassas, VA, USA) were investigated using the colony forming units (CFUs) counting technique. MCSNs and Ag-MCSNs were mixed with a 1 mL culture of *E. faecalis* (1×10^4 colony forming units [CFUs]/mL) and incubated at 4 °C for 24 h. The inoculums were then plated in 10 μL on brain heart infusion broth agar (BHI) (Oxoid, Hampshire, UK) and cultured for 24 h at 37 °C. As a negative control, bacteria inoculum devoid of nanoparticles was employed. After the test had been carried out six times for each group, *E. faecalis* CFUs were counted for group comparisons.

2.6. Cytotoxicity

MTT 3-(4,5-dimethylthiazol-2-yl)-2,5-diphenyltetrazolium bromide was dissolved in Dulbecco's phosphate buffered saline (DPBS) at pH 7.4 (5 mg/mL) to create MTT solution. Through a 0.2-m filter and into a sterilized, light-protected container, this solution was filtered and sterilized. MTT solution was kept in dark, −20 °C environment until analysis. In a ventilated fume hood, a solubilization solution was made using

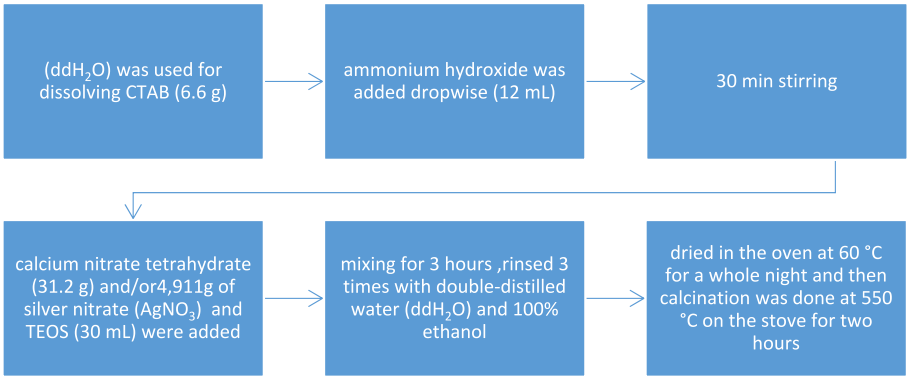

Fig. 1. Flowchart of template technique for synthesis of MCSNs and Ag-MCSNs.

40% (v/v) DMF and 2% (v/v) glacial acetic acid. This solution's pH was raised to 4.7 and SDS (16% [w/v]) was added. Storage of the solubilization solution at room temperature to stop SDS from precipitating. Cell suspensions containing MCSNs and Ag-MCSNs nanoparticles were seeded onto 96-well plates (100 μl/well) and cultured at 37 °C in a humid incubator with 5% CO_2 for 24 h, 72 h, and 168 h. A 10 μl MTT solution was added to each well, and it was then incubated at 37 °C for 1–4 h with a final concentration of 0.45 mg/mL. Following incubation, 100 μl of solubilization solution was added to the formazan crystals, and an optical multiplate reader was used to detect the absorbance at 570 nm (Spectramax 190, Molecular Devices, USA). As controls, cells that weren't exposed to the nanoparticles were employed. Three copies of the optical density (OD) findings were collected. The percentage of cell viability was calculated using the following equation:

$$\% \text{ Viability} = \text{Mean OD sample}/\text{Mean OD blank} \times 100 \quad (1)$$

2.7. Statistical analysis

The data were presented as means with standard deviations (SD) and analyzed using SPSS 26.0 using One-Way ANOVA and Tuckey and Dunnetts Post Hoc test (SPSS Inc., Chicago, IL). The significance level was set at $p < 0.05$.

3. Results and discussion

3.1. Characterizations of MCSNs and Ag-MCSNs

3.1.1. FTIR

The FTIR spectrum revealed that both MCSN and Ag-MCSN had an absorption peak at 3485 cm^1, which represents the hydroxyl group specific adsorption peak (–OH). The carbon–carbon double bonds (C]C) caused absorption peaks at 1483 and 1643 cm^1, while the deformation vibration of –OH caused an absorption peak at 1419 cm^1. All 1080, 860, 960, and 460 cm^{-1} absorption bands are assignable to Si–O–Si dissymmetrical stretching vibration, Si–O–Si symmetrical stretching vibration, Si–OH stretching vibration, and Si–O–Si bending vibration, indicating the presence of silicon skeleton structure in MCSNs and Ag-MCSNs, respectively (Fig. 2a and b).

FTIR identified that both MCSNs and Ag-MCSNs displayed hydroxyl group-specific absorption peaks, as well as other absorption peaks, which indicated the presence of silicon skeleton structure.

3.1.2. XRD

Between 20 and 30 regions showed an amorphous hump, which is attributable to hydrated silica. The findings demonstrate a significant diffraction peak at 20 = 2 in MCSNs, proving the existence of an ordered mesostructure in both MCSNs and Ag-MCSNs. Moreover, the CS hydrate and b-dicalcium silicate (b-Ca_2SiO_4) are represented by the CS diffraction peak at 20 = 29.4 and 32–34, respectively. The MCSN and Ag-MCSN wide angle XRD patterns exhibit a broad peak at around 30. (Fig. 3 a &b).

XRD identified that The major component of MCSNs was amorphous $CaSiO_3$, and neither the produced MCSNs nor the Ag-MCSNs powders included any crystalline impurities, such as CaO.

3.1.3. EDS

The elements Ca, Si, and O were found in MCSN and Ag, Ca, Si, and O elements were found in Ag-MCSN, according to EDS analysis. The ratio of each component is displayed in (Fig. 4), which also provides the percentages of Ca, Si, O, and Ag in the materials.

3.1.4. DLS

The effective diameter of MCSNs (152.3 nm) and Ag-MCSNs (177.9 nm) after being polydispersed in water with a polydispersity of (0.005) at 25 °C temperature was revealed by DLS analysis using particle size analyzer.

3.1.5. BET

The MCSNs and Ag-MCSNs' N_2 adsorption-desorption investigations revealed the distribution of pores and *type IV* isotherm pattern in the 3.7–7.15 nm range, which supported the establishment of a mesoporous reactive layer at the particle surface, a common feature of a mesoporous structure. The mesopore size of MCSN on average is 7.15 nm, and the pore volume and specific surface area of MCSNs particles are 362 $m^2\ g^{-1}$ and 0.648 $cm^3\ g^{-1}$, respectively. While The average mesopore size of Ag-MCSN is 3.7 nm, and they have specific surface areas and pore volumes of 126.25 $m^2\ g^{-1}$ and 0.117 $cm^3\ g^{-1}$, respectively (Table 1).

High surface area, large pore volume, and a steady mesopore size distribution were all validated by N_2 adsorption-desorption studies.

3.1.6. FE-SEM

The FE-SEM at various magnifications showed that MCSNs and Ag-MCSNs had spherical shapes, with nanoparticle diameters ranging from 100 to 350 nm. (Fig. 5a and b).

3.2. Ion release and pH change over time

Over nine days in Tris-HCl, it was discovered that all nanoparticles had a sustained release of the ions Ca^{2+} and Si^{4+}. Over time, the Ag-MCSNs discharged Ag^+ in addition to the earlier ions (Fig. 6). The Ca^{2+} and Si^{4+} release rates of the nanoparticles were altered by the presence of metal ions in Ag- MCSNs. Ag-MCSNs released a smaller amount of Ca^{2+} and Si^{4+} than MCSNs did. Ca^{2+} was released in bursts by both MCSNs and Ag-MCSNs during the first three days, after which the curve flattened and slightly decreased. In contrast, Si^{4+} was released steadily by both MCSNs and Ag-MCSNs for over nine days. Ag^+ release from Ag-MCSNs was growing until day 3, then it began to slightly

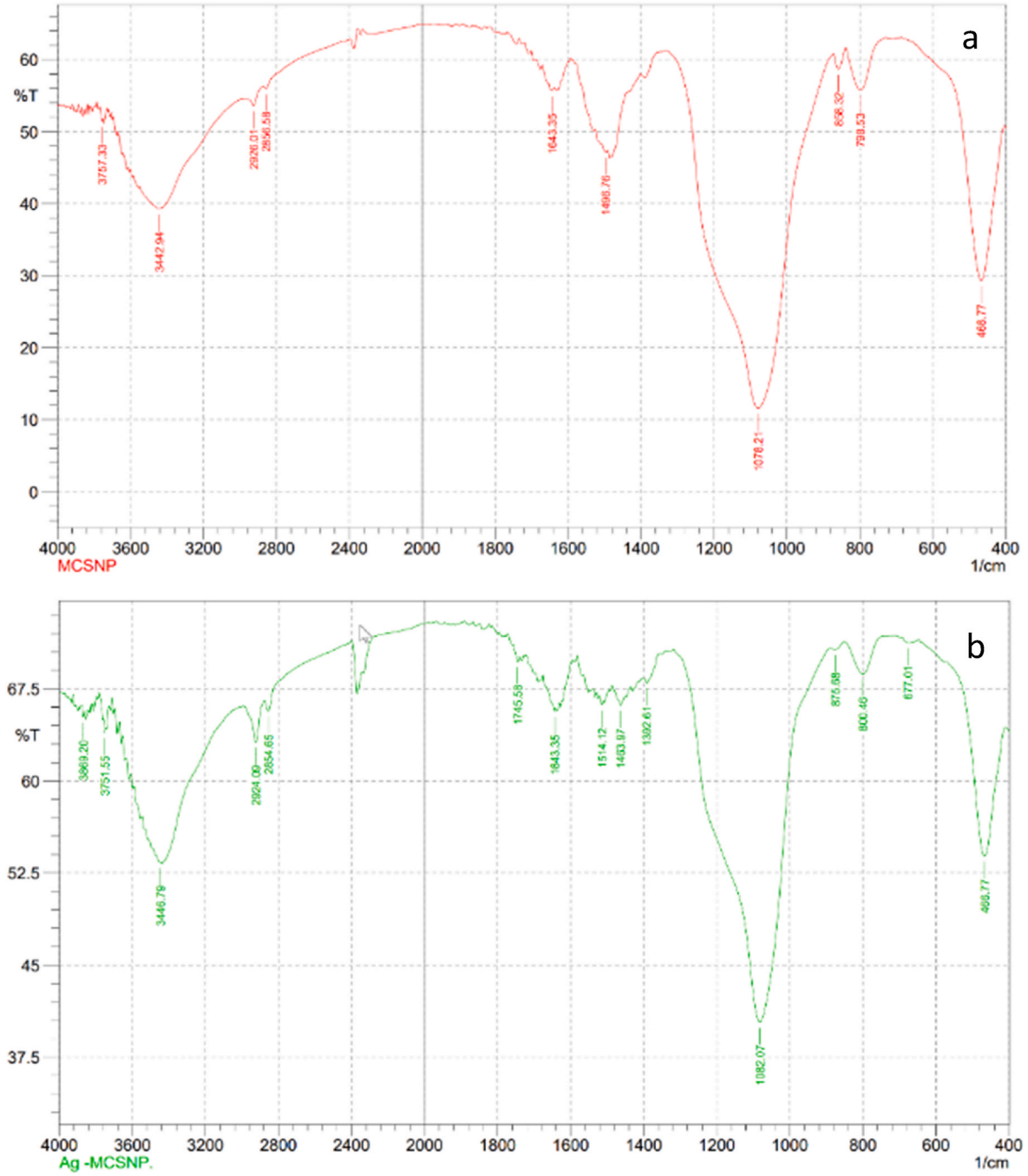

Fig. 2. FTIR spectra of MCSNs (a) and Ag-MCSNs(b).

decrease in the next 6 days. In Tris-HCl, it was discovered that all nanoparticles had a continuous release of ions.

During nine days, the pH of the MCSN and Ag-MCSN steadily increased, peaking at 9.0 and essentially remaining steady at 8.2. (Fig. 7). All solutions had an alkaline pH, and MCSNs always had a slightly higher pH than Ag-MCSNs. The pH of the MCSNs was not appreciably changed by the addition of Ag. The results showed that the pH and osmotic pressure of the solution may rise due to the nanoparticles' release of ions since the pH was always slightly higher for MCSNs than Ag-MCSNs in all experimental solutions.

3.3. Antibacterial effect of nanoparticles against E. faecalis

Many bacteria were seen on the BHI agar plate in the negative control group. Although Ag-MCSNs have shown more antimicrobial activity than MCSNs, both MCSNs and Ag-MCSNs had an antibacterial impact against *E. faecalis* ($p < 0.05$) (Fig. 8).

3.4. Cytotoxicity

Human Dermal Fibroblast: (HDFn Cell Line, Neonatal) did not exhibit observable cytotoxicity after 24 h of incubation in the presence of MCSNs or Ag-MCSNs ($p > 0.05$). Ag-MCSNs demonstrated distinct cytotoxicity to HDFn Cells after 72 h of incubation. MCSNs significantly suppressed cell growth ($p < 0.05$), even though to a lesser extent than Ag-MCSNs. The findings after 168 h of incubation were identical to those of 72 h (Fig. 9).

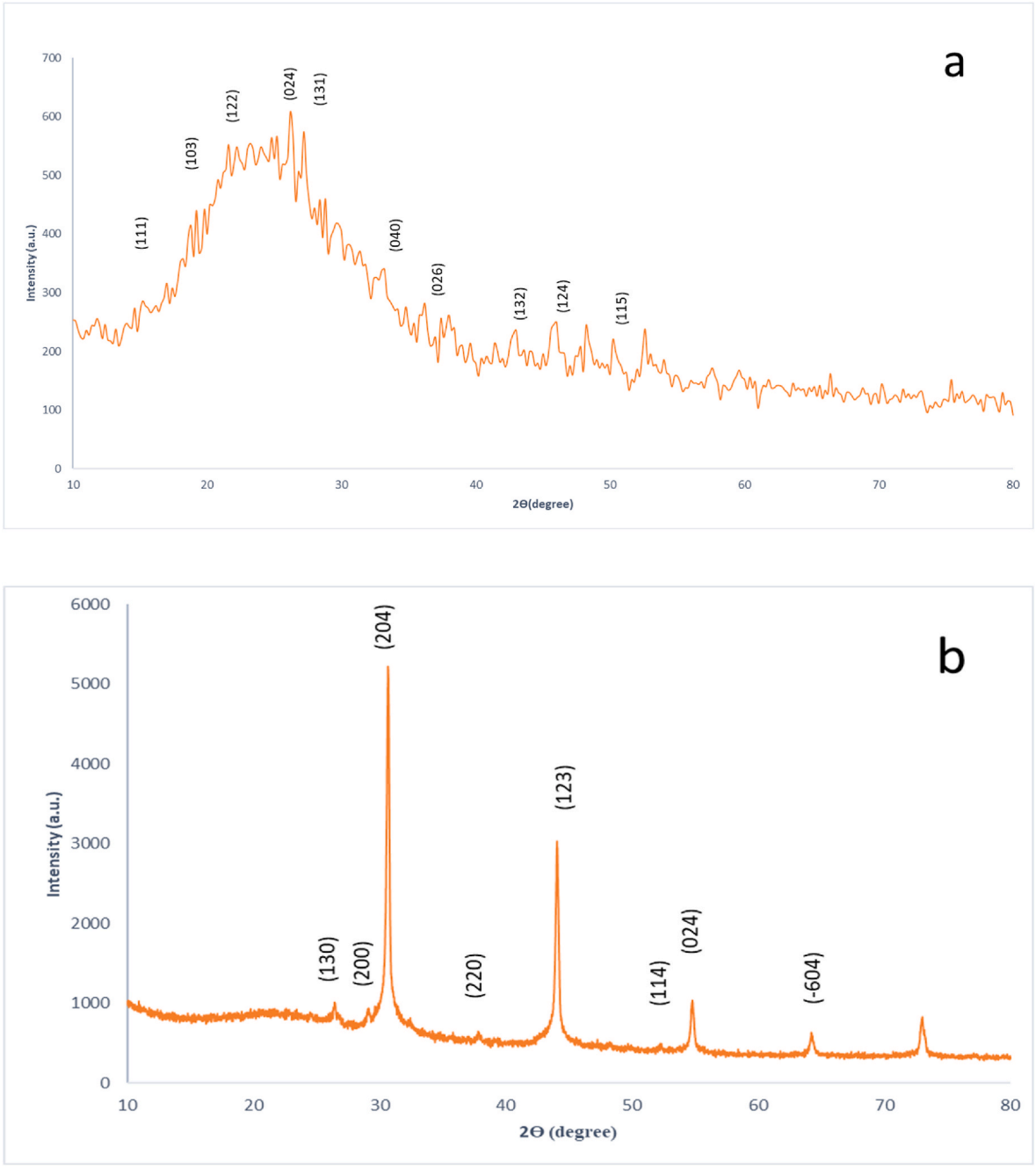

Fig. 3. The wide angle XRD pattern of nanoparticles. (a) MCSNs, (b) Ag-MCSNs.

4. Discussion

This study successfully used a synthesis technique to create new MCSNs nanoparticles. The creation of the MCSNs can be summed up as follows. At the stirring step, the capillary effect causes the ethanolic Ca $(NO_3)_2$ solution to fill the mesoporous silica pore channels. After the ethanol solvent has volatilized as $Ca(NO_3)_2$ dries, it is supported by the SBA-15 structure. $Ca(NO_3)_2$ is decomposed into CaO during the following firing process at temperatures over 470 °C, at which point it is distributed broadly throughout the pore channels of SBA-15. As the firing temperature rises, the reaction between CaO and amorphous mesoporous silica produces $CaSiO_3$ [13,14]. Through the use of the template method, the nanosilver was successfully incorporated into MCSNs. Si (TEOS) and metal elements, namely, Ca (from Ca $(NO_3)_2$) and Ag (from $AgNO_3$), interacted and combined using the CTAB as a template to construct the skeleton of mesoporous structures. Although not well explored at this time, the method of production of templated nanosilver MCSNs (Ag-MCSNs) may be comparable to that of MCSNs. Ag-MCSNs nanoparticles, like MCSNs, displayed a typical mesoporous structure, and the nanosilver was equally disseminated within the mesoporous structure [15]. Although the molecular mechanism for the coupling of MCSNs and Ag-MCSNs is not fully known, the active sites of the Ca–OH and Si–OH groups will probably link together through a covalent binding process when the mixture is heated and stirred [16,17]. The in vitro and in vivo studies corroborate a prior literature claim that the bioactivity of CS results from the formation of Si–OH on its surface upon exposure to physiological fluids [,18,19,[20]21]. In the chain silicate mineral CS, Ca^{2+} cations disrupt and modify a network of covalently attached silica molecules [22,23]. This weakly bound, network-modifying Ca^{2+} is released into the solution when hydrogen

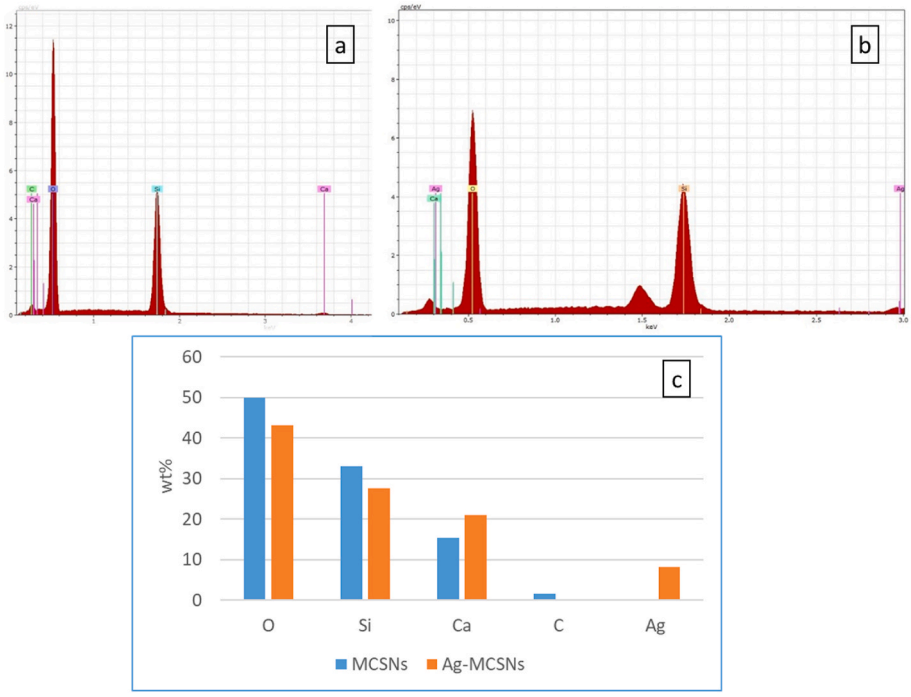

Fig. 4. EDS analysis of (a) MCSNs, (b) Ag-MCSNs, (c) Bar chart of elements proportion of MCSNs, Ag-MCSNs according to EDS analyses.

Table 1
Surface area (S_{BET}), pore volume (V_P), and mean pore size (D_P) of the nanoparticles.

Material	S_{BET} ($m^2\ g^{-1}$)	V_P ($cm^3\ g^{-1}$)	D_P (nm)
MCSNs	362	0.648	7.15
Ag-MCSNs	126.25	0.117	3.7

Abbreviations: MCSNs, mesoporous calcium-silicate nanoparticles. Ag-MCSNs, nanosilver-incorporated MCSNs.

ions are exchanged for them, ultimately leading to the formation of Si–OH. The template method of incorporating nanosilver into mesoporous nanoparticles allowed for the prolonged release of Ag^+ [24,25].

The adsorption (A) approach and the template (T) method can both be used to make MCSNs and Ag-MCSNs. Both Ag-MCSN variations displayed sustained ion release over time and exhibited the typical shape of mesoporous materials. Although Ag^+ was continuously released from Ag-MCSNs-A and Ag-MCSNs-T throughout time, the rate of release was much slower for Ag-MCSNs-T than it was for Ag-MCSNs- Because root canal disinfection relies heavily on the sustained release of antimicrobial agent, Ag-MCSNs-A and Ag-MCSNs-T may be particularly well-suited for this purpose. When compared to MCSNs with adsorbed nanosilver, those with templated nanosilver are predicted to have a more sustained antibacterial effect. Time-released Ca^{2+} and SiO_3^{2-} from Ag-MCSNs nanoparticles have been shown to aid in biomineralization and hard tissue regeneration [26]. Although Ag-MCSNs-A released more Ag^+ in a shorter amount of time than the Ag-MCSNs-T, the latter showed more cytotoxicity. These results suggest that Ag-MCSNs-T, which provides a sustained release of Ag^+ and little cytotoxicity, may be preferable for intracanal disinfection [9].

A template method was used to successfully create MCSNs and Ag-MCSNs. The Ag-MCSNs are distinguished by their mesoporous structure, in which the nano-silver is uniformly distributed. Because all manufactured particles were nanoscale, it was simple to produce an injectable paste to use in various root canal therapy methods. Moreover, mesoporous materials are advantageous because of their great surface area and pore volume, which may be used to include bioactive chemicals and medicines with antibacterial capabilities, creating multifunctional

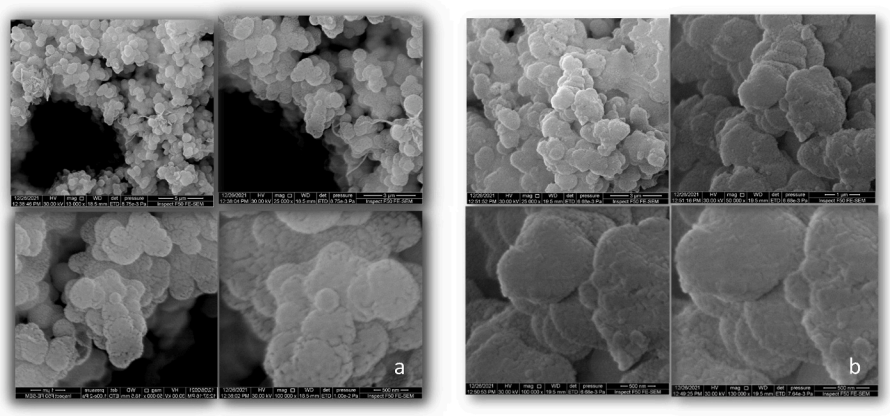

Fig. 5. FE-SEM images of the nanoparticles. (a) MCSNs, (b) Ag-MCSNs.

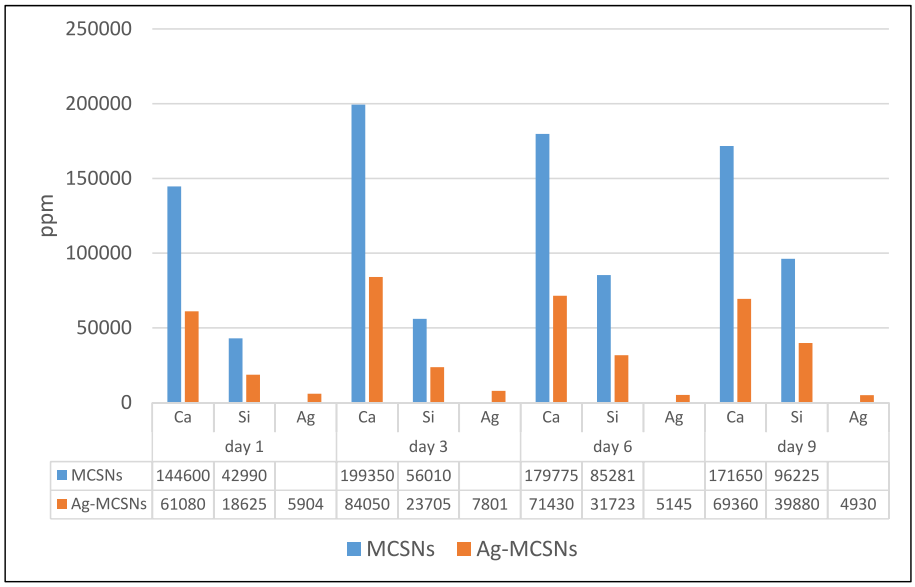

Fig. 6. Bar chart of ion release profile of MCSNs and Ag-MCSNs.

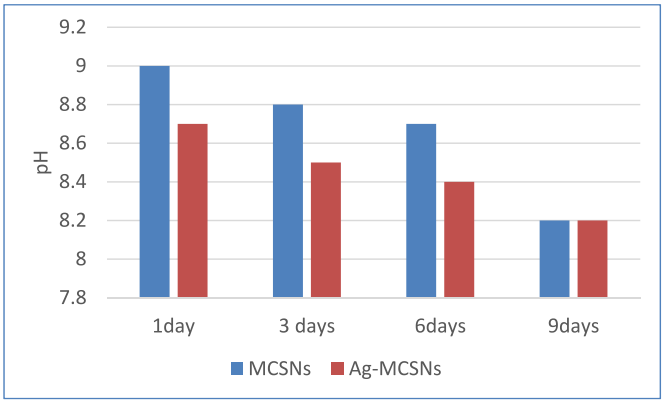

Fig. 7. Bar chart of pH measurement of MCSNs and Ag-MCSNs.

biomaterials.

All nanoparticles in this study were able to release Ca^{2+}, Si^{4+}, and Ag^{+}, which created a mildly alkaline microenvironment and sustained an acceptable pH value throughout time. FTIR, XRD, EDS, DLS, BET, and FE-SEM were used to make these discoveries. These features are compatible with earlier research on materials made of calcium silicate [27–29]. FTIR and XRD identified that both MCSNs and Ag-MCSNs displayed hydroxyl group-specific absorption peaks, as well as other absorption peaks, which indicated the presence of silicon skeleton structure. The major component of MCSNs was amorphous $CaSiO_3$, and neither the produced MCSNs nor the Ag-MCSNs powders included any crystalline impurities, such as CaO.

High surface area, large pore volume, and a steady mesopore size distribution were all validated by N_2 adsorption-desorption studies, proving that MCSNs and Ag-MCSNs containing CS had mesoporous structures. As a consequence, two characteristics are shared by the prepared MCSNs and the Ag-MCSNs. For *one*, they're on the nanoscale. They may simply be made into an injectable paste to plug the root canal at the tooth's apex. The *other* is that they may be used to deliver antibacterial medications because of their great pore volume and surface area. Numerous investigations have shown that CTAB may be used as a template for the synthesis of pure mesoporous SiO_2 nanoparticles with a surface area of up to 1000 $m^2\ g^{-1}$ [30,31]. Although mesoporous SiO_2 nanoparticles have a large surface area, they are unable to form apatite in biological fluids [32,33]. According to our research, it is possible to make mesoporous Ca–Si nanoparticles using a simple CTAB template approach. The generated MCSNs have high surface area and pore volume while having smaller pore sizes than mesoporous SiO_2 nanoparticles. Many biomolecules, including drugs, antibiotics, and growth hormones, are considered adsorbed most efficiently at a surface area of 200–350 $m^2\ g^{-1}$, with a mesopore size of 3–5 nm [34]. The high surface area of MCSNs (362 $m^2\ g^{-1}$) comes nearly perfectly inside the ideal surface area range shown above. As a result, MCSNs may be used to transport pharmaceuticals to the patient.

Well-organized nanopores and channel structures were seen in the mesoporous architectures of both MCSNs and Ag-MCSNs, and the latter included numerous Ag particles, according to FE-SEM images.

In Tris-HCl, it was discovered that all nanoparticles had a continuous release of ions. Tris-HCl was used as the solution for the ion release profile because the medium affected the ion release. Ion exchange could be delayed by a more complicated medium. Ion release would be less inhibited by the presence of extra ions in dilute solutions like Tris-HCl. For example, in SBF, although the Si^{4+} release accelerated, the Ca^{2+} release slowed due to the greater Ca^{2+} concentration in the solution. Nevertheless, alpha minimum essential medium (α-MEM) similarly inhibited the release of Ca^{2+} from particles despite having a lower Ca^{2+} concentration than in SBF. This could be brought on by the biological components in α-MEM [35–37]. Ca^{2+} and Si^{4+} were emitted from every nanoparticle. Over time, in addition to the earlier ions, the Ag-MCSNs discharged Ag^{+}. These results were agreed with previous studies [8,9].

The results showed that the pH and osmotic pressure of the solution may rise due to the nanoparticles' release of ions since the pH was always slightly higher for MCSNs than Ag-MCSNs in all experimental solutions. The surface Ca^{2+} cations of MCSNs may operate as the natural active site for the efficient adsorption of Ag^{+} to –OH groups [38]. The aforementioned hypothesis may also help to explain why Ag-MCSNs release less Ca^{2+} and have a relatively lower pH value than MCSNs. Ag^{+} is projected to bind to the Si^{4+} skeleton of the mesoporous structures since the –OH groups of MCSNs are commonly connected to Si^{4+}. This may help to explain why Si^{4+} is released from MCSNs more frequently than from Ag-MCSNs [37]. Keeping Ca^{2+} and Si^{4+} in the environment would promote mineralization and crystallization which is thought to be a crucial characteristic of in vivo bone regeneration [35, 36].

Ag-MCSNs nanoparticles significantly outperformed MCSNs in the planktonic antibacterial test, demonstrating that the antibacterial action

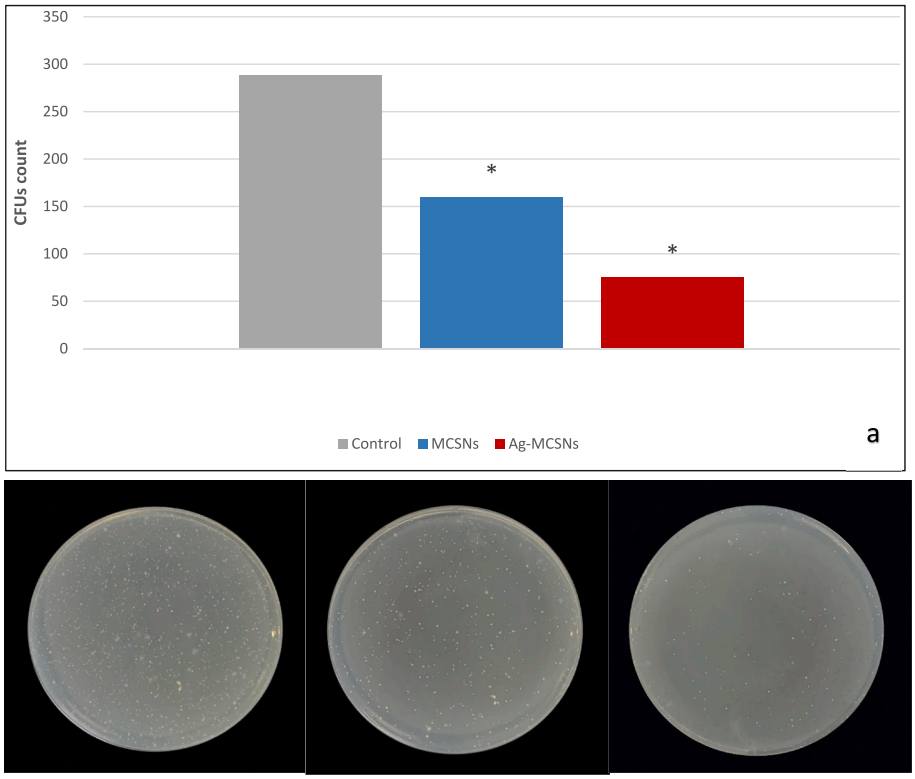

Fig. 8. Antibacterial effect of materials against planktonic *E. faecalis*. (a) Bar chart for comparison of CFU count among groups *p < 0.05 when compared with control group, (b) negative control, (c) MCSNs, (d) Ag-MCSNs.

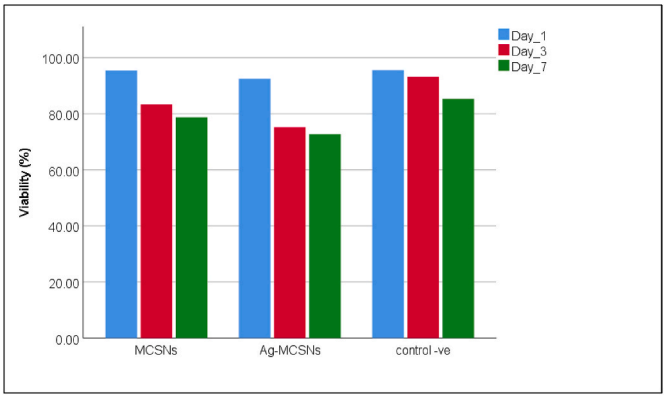

Fig. 9. Bar chart of MTT assay test on the HDFn Cell.

of Ag-MCSNs is connected to the discharged Ag^{+} rather than the Ca^{2+} or Si^{4+}. Ag^{+}, which is produced by Ag-MCSNs, may directly harm bacterial cell walls and membranes and penetrate the cells, leading to the leakage of cell contents and the obliteration of intracellular structures, both of which result in the death of the bacteria. Ag^{+} has a strong attraction for electron-giving groups, such as sulfhydryl, carbonyl, amino, imidazole, and phosphate groups, which are widely present in proteins or cell membranes. Ag^{+} may attach to proteins' thiol groups (ASH) to form stable AS-Ag bonds, which can alter the proteins' three-dimensional (3D) structure and obstruct the active binding sites [39,40]. The high reactivity of Ag^{+} may bind to tissue proteins and alter the structure of bacterial cell walls and nuclear membranes, resulting in cell deformation and death. By attaching to bacterial DNA and RNA, Ag^{+} may also denature and prevent bacterial reproduction [41]. Compared to the blank control, the MCSNs also showed little antibacterial effect. Yet, it is unclear what causes MCSNs to have antibacterial action against planktonic *E. faecalis*. One reason is that the Si^{4+} and Ca^{2+} that are produced create an alkaline microenvironment [42]. Moreover, MCSNs' Nano dimensions may disrupt bacterial metabolism, particularly when the nanoparticles come into touch with the bacteria directly in a liquid environment [43,44]. In this study, MCSNs showed a slight antibacterial effect, which agrees with previous study [15].

Cell proliferation was greatly slowed down by MCSNs and Ag-MCSNs. The findings revealed that the cytotoxicity relies on the quantity and duration of Ag exposure, the longer the period of Ag, the greater the cytotoxicity. The Ag-MCSNs showed increased cytotoxicity compared to MCSNs. These results were consistent with earlier research showing the harmful impacts of Ag on human health [45]. However, both nanoparticles are considered noncytotoxic. According to the UNI EN ISO 10993/2009 regulation that outlines how to conduct the biological assessment of medical devices, a sample is termed non-cytotoxic if the percentage vitality value is >70% and cytotoxic if the percentage vitality value is 70%. Section 5 in particular provides detailed instructions for in vitro techniques to assess the cytotoxicity of various compounds [46,47].

5. Conclusion

A template method was successfully used to create bioactive MCSNs particles with a nanoscale size within the parameters of this investigation. The internal architecture of the particles is a mesoporous network with a large specific surface area and pore volume. Nano-silver can be effectively integrated into MCSNs like that of Ag-MCSNs. Several chemical and structural characterization techniques were used to demonstrate these conclusions. Both materials displayed ion release, alkaline pH (8.2–9.0), minimal cytotoxicity (vitality value is >70%), and outstanding antibacterial performance with MCSNs containing Ag (Ag-MCSNs) showing higher antibacterial effect. This substance may be improved to provide a better root canal filler material, sealer, or novel intracanal medicament in dentistry.

Funding statement

This research did not receive any specific grant from funding agencies in the public, commercial, or not-for-profit sectors. The study is self-funded.

CRediT authorship contribution statement

Amer A. Mohammed: Writing – original draft, Resources, Methodology, Investigation. **Ahmed H. Ali:** Supervision.

Declaration of competing interest

The authors declare that they have no known competing financial interests or personal relationships that could have appeared to influence the work reported in this paper.

Data availability

Data will be made available on request.

References

[1] J. Jeevanandam, A. Barhoum, Y.S. Chan, A. Dufresne, M.K. Danquah, Review on nanoparticles and nanostructured materials: history, sources, toxicity and regulations, Beilstein J. Nanotechnol. 9 (2018) 1050–1074.
[2] I. Khan, K. Saeed, I. Khan, Nanoparticles: properties, applications and toxicities, Arab. J. Chem. 12 (7) (2019) 908–931, https://doi.org/10.1016/j.arabjc.2017.05.011.
[3] N. Beyth, Y. Houri-Haddad, A. Domb, W. Khan, R. Hazan, Alternative Antimicrobial approach: nano-antimicrobial materials, Evid. Based Complement. Alternat. Med. 2015 (2015) 246012.
[4] Jasmine Wong, Ting Zou, Angeline Hui, Cheng Lee, Chengfei Zhang, The potential translational applications of nanoparticles in endodontics, Int. J. Nanomed. 16 (2021) 2087–2106.
[5] Ching-Yuang Huang, Tsui-Hsien Huang, Chia-Tze Kao, Yuan-Haw Wu, Wan-Chen Chen, Ming-You Shie, Mesoporous calcium silicate nanoparticles with drug delivery and odontogenesis properties, Am. Assoc. Endodont. 43 (2017). Number 1, January.
[6] M.S. Islam, H.N. Choi, W.S. Choi, H.J. Lee, Polyelectrolyte-mediated hierarchical mesoporous calcium silicates: a platform for drug delivery carrier with ultrahigh loading capacity and controlle release behavior, J. Mater. Chem. B 3 (2015) 1001–1009.
[7] Y.F. Shen, C.C. Ho, M.Y. Shie, et al., Hinokitiol-loaded mesoporous calcium silicate nanoparticle induce apoptotic cell death through regulation of the function of MDR1 in lung adenocarcinoma cells, Materials 9 (2016) 306.
[8] Jie Zhu, Ruizhen Liang, Chao Sun, Lizhe Xie, Juan Wang, Diya Leng, Daming Wu, Weihong Liu, Effects of nanosilver and nanozinc incorporated mesoporous calcium-silicate nanoparticles on the mechanical properties of dentin, PLoS ONE 12 (8) (2017) e0182583.
[9] Wei Fan, Daming Wu, Franklin R Tay2 Tengjiao, Ma1 Yujie Wu1 Bing Fan1 Effects of adsorbed and templated nanosilver in mesoporous calcium-silicate nanoparticles on inhibition of bacteria colonization of dentin, Int. J. Nanomed. 9 (2014) 5217–5230.
[10] M. Ahamed, M. Karns, M. Goodson, et al., DNA damage response to different surface chemistry of silver nanoparticles in mammalian cells, Toxicol. Appl. Pharmacol. 233 (3) (2008) 404–410.
[11] A.H. Ali, A.F. Mahdee, N.H. Fadhil, D.M. Shihab, Prevalence of periapical lesions in non-endodontically and endodontically treated teeth in an urban Iraqi adult subpopulation: a retrospective CBCT analysis, J. Clin. Exp. Dent. 14 (11) (2022) e953–e958.
[12] W. Fan, D. Wu, F.R. Tay, T. Ma, Y. Wu, B. Fan, Effects of adsorbed and templated nanosilver in mesoporous calcium-silicate nanoparticles on inhibition of bacteria colonization of dentin, Int. J. Nanomed. 9 (2014) 5217–5230.
[13] Y.J. Zhu, X.X. Guo, T.K. Sham, Calcium silicate-based drug delivery systems, Expet Opin. Drug Deliv. 14 (2) (2017) 215–228.
[14] Li Xia, Jianlin Shi, Yufang Zhu, Weihua Shen, Hua Li, Jian Liang, Jianhua Gao, A template route to the preparation of mesoporous amorphous calcium silicate with high in vitro bone-forming bioactivity, J. Biomed. Mater. Res. Part B: Appl. Biomater. 83B (2007) 431–439.
[15] Wei Fan, Daming Wu, Franklin R Tay 2 Tengjiao Ma1 Yujie Wu1 Bing Fan. Effects of adsorbed and templated nanosilver in mesoporous calcium-silicate nanoparticles on inhibition of bacteria colonization of dentin, Int. J. Nanomed. 9 (2014) 5217–5230.
[16] W. Fan, Y. Li, Q. Sun, T. Ma, B. Fan, Calcium-silicate mesoporous nanoparticles loaded with chlorhexidine for both anti Enterococcus faecalis and mineralization properties, J. Nanobiotechnol. 14 (2016) 1–12.
[17] X. Guo, Z. Wang, J. Wu, Y.-M. Yiu, Y. Hu, Y.-J. Zhu, T.-K. Sham, Tracking drug loading capacities of calcium silicate hydrate carrier: a comparative X-ray absorption near edge structures study, J. Phys. Chem. B 119 (2015) 10052–10059.
[18] P.N. De Aza, F. Guitian, S. De Aza, Bioactivity of wollastonite ceramics: in vitro evaluation, Scripta Metall. Mater. 31 (1994) 1001–1005.
[19] P.N. De Aza, Z.B. Luklinska, A. Martinez, M.R. Anseau, F. Guitian, S. De Aza, Morphological and structural study of pseudowollastonite implants in bone, J. Microsc. 197 (2000) 60–67.
[20] X.Y. Liu, C.X. Ding, Z.Y. Wang, Apatite formed on the surface of plasma-sprayed wollastonite coating immersed in simulated body fluid, Biomaterials 22 (2001) 2007–2012.
[21] W.C. Xue, X.Y. Liu, X.B. Zheng, C.X. Ding, In vivo evaluation of plasma-sprayed wollastonite coating, Biomaterials 26 (2005) 3455–3460.
[22] W.H. Casey, H.R. Westrich, J.F. Banfield, G. Ferruzzl, G.W. Arnold, Leaching and reconstruction at the surfaces of dissolving chain silicate minerals, Nature 366 (1993) 253–256.
[23] E.J. Weissbart, J.D. Rimstidt, Wollastonite: incongruent dissolution and leached layer formation, Geochem. Cosmochim. Acta 64 (2000) 4007–4016.
[24] A.M. El-Kady, A.F. Ali, R.A. Rizk, M.M. Ahmed, Synthesis, characterization and microbiological response of silver doped bioactive glass nanoparticles, Ceram. Int. 38 (1) (2012) 177–188.
[25] S. Shruti, A.J. Salinas, G. Lusvardi, G. Malavasi, L. Menabue, M. Vallet-Regi, Mesoporous bioactive scaffolds prepared with cerium-, gallium- and zinc-containing glasses, Acta Biomater. 9 (1) (2013) 4836–4844.
[26] C. Wu, J. Chang, W. Fan, Bioactive mesoporous calcium-silicate nanoparticles with excellent mineralization ability, osteostimulation, drug-delivery and antibacterial properties for filling apex roots of teeth, J. Mater. Chem. 22 (2012) 16801–16809.
[27] Q. Sun, M. Duan, W. Fan, B. Fan, Ca–Si mesoporous nanoparticles with the optimal Ag–Zn ratio inhibit the Enterococcus faecalis infection of teeth through dentinal tubule infiltration: an in vitro and in vivo study, J. Mater. Chem. B 9 (2021) 2200–2211.
[28] A.M. Brezoiu, M. Prundeanu, D. Berger, M. Deaconu, C. Matei, O. Oprea, E. Vasile, T. Negreanu-Pirjol, D. Muntean, C. Danciu, Properties of Salvia officinalis L. And thymus serpyllum L. Extracts free and embedded into mesopores of silica and Titania nanomaterials, Nanomaterials 10 (2020) 820.
[29] V. Buda, A.-M. Brezoiu, D. Berger, I. Pavel, D. Muntean, D. Minda, C. Dehelean, C. Soica, Z. Diaconeasa, R. Folescu, et al., Biological evaluation of black Chokeberry extract free and embedded in two mesoporous silica-type matrices, Pharmaceutics 12 (2020) 838.
[30] H.S. Yun, S.H. Kim, S. Lee, I.H. Song, Mater. Lett. 64 (2010) 1850–1853.
[31] M. Vallet-Regi, A. Ramila, R.P. del Real, J. Perez-Pariente, Chem. Mater. 13 (2001) 308–311.
[32] P. Horcajada, A. Ramila, K. Boulahya, J. Gonzalez-Calbet, M. Vallet-Regi, Solid State Sci. 6 (2004) 1295–1300.
[33] Izquierdo-Barba, L. Ruiz-Gonzalez, J.C. Doadrio, J.M. Gonzalez Calbet, M. Vallet-Regi, Solid State Sci. 7 (2005) 983–989.
[34] M. Vallet-Regi, F. Balas, D. Arcos, Angew. Chem., Int. Ed. 46 (2007) 7548–7558.
[35] Y. Pu, Y. Huang, S. Qi, C. Chen, H.J. Seo, In situ hydroxyapatite nanofiber growth on calcium borate silicate ceramics in SBF and its structural characteristics, Mater. Sci. Eng., C 55 (2015) 126–130.
[36] X. Wang, Y. Zhou, L. Xia, C. Zhao, L. Chen, D. Yi, J. Chang, L. Huang, X. Zheng, H. Zhu, et al., Fabrication of nano-structured calcium silicate coatings with enhanced stability, bioactivity and osteogenic and angiogenic activity, Colloids Surf. B Biointerfaces 126 (2015) 358–366.
[37] Wei Fan, Yanyun Li, Qing Sun, Tengjiao Ma, Bing Fan, Calcium-silicate mesoporous nanoparticles loaded with chlorhexidine for both anti- Enterococcus faecalis and mineralization properties, J. Nanobiotechnol. 14 (2016) 72.
[38] Y.-J. Zhu, X.-X. Guo, T.-K. Sham, Calcium silicate-based drug delivery systems, Expet Opin. Drug Deliv. 14 (2016) 215–228.
[39] S. Tang, J. Zheng, Antibacterial activity of silver nanoparticles: structural effects, Adv. Healthcare Mater. 7 (13) (2018) e1701503, 201701503.
[40] D.J. Kadhem, A.H.M. Al Haidar, Antibacterial and cytotoxic effect of a novel biological Nano-silver fluoride synthesized from moringa oleifera leaf extract, J. Bagh. Coll. Dent. 35 (2) (2023) 32–44.
[41] A. Pugazhendhi, D. Prabakar, J.M. Jacob, et al., Synthesis and characterization of silver nanoparticles using Gelidium amansii and its antimicrobial property against various pathogenic bacteria, Microb. Pathog. 114 (2018) 41–45, 2017.11.013.
[42] S. Shruti, A.J. Salinas, G. Lusvardi, G. Malavasi, L. Menabue, M. Vallet-Regi, Mesoporous bioactive scaffolds prepared with cerium-, gallium- and zinc-containing glasses, Acta Biomater. 9 (1) (2013) 4836–4844.
[43] G. Mohammadi, H. Valizadeh, M. Barzegar-Jalali, et al., Development of azithromycin-PLGA nanoparticles: physicochemical characterization and antibacterial effect against Salmonella typhi, Colloids Surf. B Biointerfaces 80 (1) (2010) 34–39.
[44] Ahmed I Al-Jobory, Raghad Al-Hashimi, Antibacterial activity of bioactive glass 45S5 and Chitosan incorporated as fillers into Gutta Percha, J. Res. Med. Dent. Sci. 9 (3) (2021) 108–117.
[45] A. Shrestha, A. Kishen, Antibacterial nanoparticles in endodontics: a review, J. Endod. 42 (10) (2016) 1417–1426, 2016. 05.021.
[46] International Organization for Standardization, Biological Evaluation of Medical Devices—Part 5: in Vitro Cytotoxicity Testing, UNI EN ISO 10993-5:2009, International Organization for Standardization, Geneva, Switzerland, 2009.
[47] L.M. brahim, R.K. Jassim, A. Al Gabban, Evaluation of cytotoxicity and biocompatibility of Ti2AlC in rabbits, J. Bagh. Coll. Dent. 33 (4) (2021) 20–24.